Polymer 51 (2010) 2540–2547

Contents lists available at ScienceDirect

Polymer

journal homepage: www.elsevier.com/locate/polymer

Fe_3O_4@poly(2-hydroxyethyl methacrylate)-*graft*-poly(ε-caprolactone) magnetic nanoparticles with branched brush polymeric shell

Weizhong Yuan [a,b], Jinying Yuan [a,*], Lilin Zhou [a], Sizhu Wu [c], Xiaoyin Hong [a]

[a] Key Lab of Organic Optoelectronics & Molecular Engineering of Ministry of Education, Department of Chemistry, Tsinghua University, Beijing 100084, People's Republic of China
[b] Institute of Nano and Bio-Polymeric Materials, School of Material Science and Engineering, Tongji University, Shanghai 200092, People's Republic of China
[c] Key Lab of Science and Technology of Controlled Chemical Reactions, Beijing University of Chemical Technology, Beijing 100029, People's Republic of China

ARTICLE INFO

Article history:
Received 17 December 2009
Received in revised form
2 April 2010
Accepted 9 April 2010
Available online 24 April 2010

Keywords:
Superparamagnetic nanoparticles
Brush polymeric shell
Degradation

ABSTRACT

Well-defined monodisperse Fe_3O_4@poly (2-hydroxyethyl methacrylate)-*graft*- poly(ε-caprolactone) (Fe_3O_4@PHEMA-*g*-PCL) magnetic nanoparticles with novel topological structure, i.e., with branched brush polymeric shell, were successfully prepared by the combination of atom transfer radical polymerization (ATRP) and ring-opening polymerization (ROP). Oleic acid stabilized monodisperse Fe_3O_4 nanoparticles were prepared by a convenient organic phase process and underwent a ligand exchange process with 2-bromo-2-methylpropionic acid (Br-MPA) to generate macroinitiator (Fe_3O_4@Br-MPA) for ATRP of 2-hydroxyethyl methacrylate (HEMA) to produce Fe_3O_4@poly(2-hydroxyethyl methacrylate) (Fe_3O_4@PHEMA). PCL segments were grafted from the side of PHEMA by the ROP of ε-caprolactone (CL) with the hydroxyl groups of PHEMA segments used as initiation centers, and then Fe_3O_4@PHEMA-*g*-PCL magnetic nanoparticles were obtained. PCL segments of Fe_3O_4@PHEMA-*g*-PCL possessed lower degree of crystallinity than that of linear PCL. Meanwhile, Fe_3O_4@PHEMA-g-PCL nanoparticles showed superparamagnetism and comparatively strong magnetization. *In vitro* degradation investigation indicated that the degradation rate of PCL segments in Fe_3O_4@PHEMA-*g*-PCL increased with the decrease of the length of PCL chains. The release behavior of model drug chlorambucil from the nanoparticles indicated that the rate of drug release could be adjusted by altering the chain-length of PCL segments.

1. Introduction

Considerable attention has been focused on the surface functionalization of inorganic nanoparticles by a polymeric shell with well-defined architecture due to the improvement of the properties of the nanoparticles, such as the dispersion and stability in various solvent [1–9]. More importantly, the nanoparticles functionalized by polymer could combine the advantages of inorganic nanoparticles and polymer materials [10–20].

Fe_3O_4 magnetic nanoparticles have been used in various fields such as sealing, oscillation damping, information storage and electronic devices [21–24]. One of the rapidly developing applications of Fe_3O_4 magnetic nanoparticles in recent years is in biomedical areas, including rapid biologic separation and drug delivery [25–28]. Surface functionality of Fe_3O_4 magnetic nanoparticles with polymeric shell is of current research interest owing to the flexibility in the control of the chemical structure, composition, and function of the polymers. Schmidt *et al.* reported the preparation of Fe_3O_4/poly(ε-caprolactone) (Fe_3O_4/PCL) core-shell particles and Fe_3O_4/poly(2-methoxyethyl methacrylate) (Fe_3O_4/PMEMA) thermoresponsive core-shell nanoparticles [29,30]. Neoh *et al.* investigated the surface functionalization of Fe_3O_4 magnetic nanoparticles via living radical graft polymerization with styrene and acrylic acid in the reversible addition-fragmentation chain transfer (RAFT)-mediated process [31]. Li *et al.* reported the preparation of Fe_3O_4 magnetic nanoparticles coated with an amphiphilic block copolymer as hydrophobic drug carriers [32].

However, Fe_3O_4/polymers magnetic nanoparticles reported by the literatures were prepared almost with the similar method: the polymers were grafted from the surface of Fe_3O_4 nanoparticles directly [33,34]. Therefore, the content of polymer in nanoparticles was limited and influenced by the number of functional groups on the surface of Fe_3O_4 nanoparticles and the steric hindrance. In order to increase the content of polymer in the nanoparticles, the long-chain polymer should be prepared. PCL is one of the most important biodegradable and biocompatible materials and have been extensively used for drug delivery systems, biodegradable sutures, and temporary scaffolding for tissue [35–44]. For PCL, the linear long-chains will lead to the high degree of crystallinity and low degradation rate. Thus the rate of drug release will be low and

* Corresponding author. Tel.: +86 10 62783668; fax: +86 10 62771149.
E-mail address: yuanjy@mail.tsinghua.edu.cn (J. Yuan).

0032-3861/$ – see front matter © 2010 Elsevier Ltd. All rights reserved.
doi:10.1016/j.polymer.2010.04.016

uncontrolled. Herein, we report a novel approach to increase the content of polymer without long-chain polymer. Firstly, a kind of polymer containing many functional groups (e.g. poly(2-hydroxyethyl methacrylate), PHEMA) was grafted from the surface of Fe_3O_4 nanoparticles, and then a number of short chains of another kind of polymer (e.g. PCL) were grafted from the first kind of polymer. The presence of many short chain polymers on the surface of nanoparticles can increase the content of polymer in nanoparticles, decrease the degree of crystallinity and increase the degradation rate compared with linear long-chain PCL.

To date, some reports have been shown for the preparation of comb-like polymer brushes on solid surface [45–48]. The work presented here demonstrated the preparation of novel, well-defined, and monodisperse Fe_3O_4@poly(2-hydroxyethyl methacrylate)-*graft*-poly(ϵ-caprolactone) (Fe_3O_4@PHEMA-*g*-PCL) magnetic nanoparticles with branched brush polymeric shell by atom transfer radical polymerization (ATRP) and ring-opening polymerization (ROP) (Scheme 1 and Scheme 2). The graft copolymer PHEMA-*g*-PCL was grafted onto Fe_3O_4 surfaces via the "grafting from" approach. The monodisperse Fe_3O_4 nanoparticles stabilized with oleic oil were synthesized by a convenient organic phase process [49]. Then these nanoparticles were underwent a ligand exchange process with 2-bromo-2-methylpropionic acid (Br-MPA) to generate macroinitiator (Fe_3O_4@Br-MPA) for ATRP of 2-hydroxyethyl methacrylate (HEMA) to produce Fe_3O_4@poly(2-hydroxyethyl methacrylate) (Fe_3O_4@PHEMA). PHEMA had accepted biocompatibility and hydroxyl groups in its side chains, which could initiate the ROP of ϵ-caprolactone (CL) to form Fe_3O_4@-PHEMA-*g*-PCL. The well-defined branched structure of PHEMA-*g*-PCL on the surface of Fe_3O_4 nanoparticles formed brush macromolecules and offered more PCL segments but shorter PCL chain length, which could decrease the degree of crystallinity and improve the biodegradability of PCL effectively. Furthermore, *in vitro* degradation and drug release of Fe_3O_4@PHEMA-*g*-PCL nanoparticles were investigated.

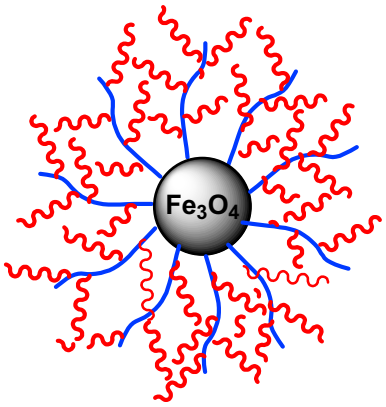

Scheme 2. Structure of Fe_3O_4@PHEMA-*g*-PCL magnetic nanoparticle with branched brush polymeric shell.

2. Experimental

2.1. Materials

Iron acetylacetonate ($Fe(acac)_3$; Acros Organic, 99+%), 1,2-dodecanediol (Aldrich, 90%), oleylamine (Aldrich, 70%), oleic acid (Aldrich, 90%), and Br-MPA (Acros Organic, 98%) were used as received. HEMA (Acros Organic, 96%) was passed through a column of oxide alumina to remove the inhibitor and distilled *in vacuo*. CL (Acros Organic, 99%) was purified with CaH_2 by vacuum distillation. Tin 2-ethylhexanoate ($Sn(Oct)_2$; Aldrich, 95%) was distilled under reduced pressure before use. Pentamethyldiethylenetriamine (PMDETA; Acros Organic, 99%) was stirred overnight over CaH_2 and distilled under reduced pressure before use. CuBr (Aldrich, 99+%) was purified via stirring in acetic acid and washing with ethanol and then dried *in vacuo*. Chlorambucil was purchased from Fluka Chemika (USA) and used directly. Methylene chloride, hexane, tetrahydrofuran (THF), and anisole were dried over CaH_2 and distilled prior to use. Diphenyl ether was used without further purification.

2.2. Characterization

Fourier transform infrared (FTIR) spectra were recorded on an Avatar 360 ESP FTIR spectrometer. Transmission electron microscopy (TEM) analysis of Fe_3O_4 magnetic nanoparticles and Fe_3O_4@PHEMA-*g*-PCL nanoparticles was performed on a JEM-2010 high resolution electron microscope at 120 kV. ^{1}H NMR and ^{13}C NMR spectra were obtained with JOEL JANM-ECA300 NMR spectrometer with $CDCl_3$ as the solvent. The chemical shifts were determined with respect to tetramethylsilane at $\delta = 0$ ppm for protons. The molecular weights and molecular weight distributions were measured on a Viscotek TDA 302 gel permeation chromatography (GPC) apparatus equipped with two columns (GMHHR-H, M mixed bed). THF was used as the eluent at a flow rate of

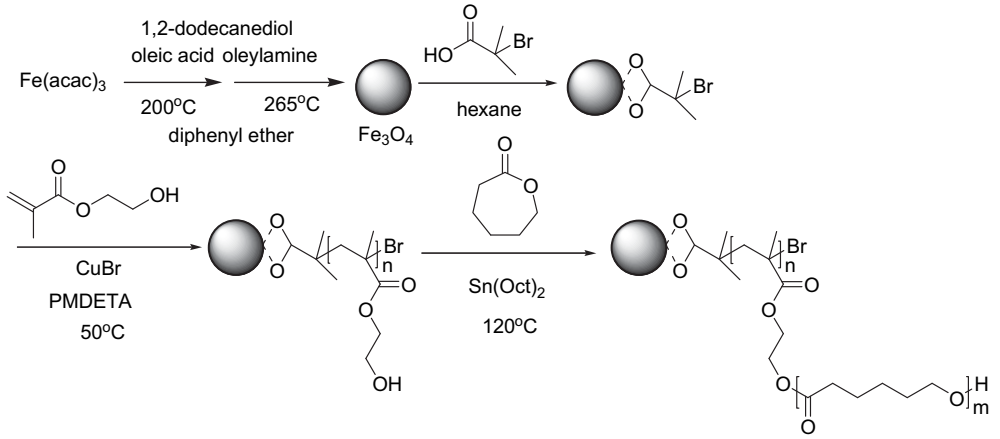

Scheme 1. Synthesis of Fe_3O_4@PHEMA-*g*-PCL magnetic nanoparticles by ATRP and ROP.

1 mL min^{-1} at 30 °C. Differential scanning calorimetry (DSC) analysis system was carried on a DSC 2910 thermal analysis system at a heating rate of 10 °C min^{-1} from 0 °C to 100 °C under a nitrogen atmosphere. Thermogravimetric analysis (TGA) was carried out on a TGA 2050 thermogravimetric analyzer with a heating rate of 20 °C min^{-1} from room temperature to 550 °C under a nitrogen atmosphere. Magnetic measurements were performed on Lakeshore 7307 VSM (Vibrating Sample Magnetometer) system at room temperature. UV spectroscopy measurements were performed on a UV 2100 UV–visible Spectrophotometer (SHIMADZU, Japan).

2.3. Synthesis of Fe_3O_4 and Fe_3O_4@Br-MPA nanoparticles

The preparation of Fe_3O_4 and Fe_3O_4@Br-MPA nanoparticles were performed according to the previous reports [32,49]. Briefly, Fe(acac)$_3$ (0.7063 g, 2 mmol), 1,2-dodecanediol (2.0234 g, 10 mmol), oleic acid (1.6948 g, 6 mmol), oleylamine (1.605 g, 6 mmol), and diphenyl ether (20 mL) were mixed and magnetically stirred under a flow of argon. The mixture was heated to 200 °C for 30 min and then heated to 265 °C for another 30 min Fe_3O_4 nanoparticles could be obtained by precipitation with ethanol and separation via centrifugation. The Fe_3O_4 nanoparticles (549.6 mg) and Br-MPA (560 mg, 3.35 mmol) were dispersed into hexane (10 mL). The mixture was stirred for 72 h at room temperature under the protection of argon. Fe_3O_4@Br-MPA nanoparticles were obtained by precipitation with ethanol and separation via centrifugation.

2.4. Synthesis of Fe_3O_4@PHEMA nanoparticles

A typical polymerization procedure was as follows: A dry Schlenk flask with magnetic stirrer was charged with CuBr (30 mg, 0.21 mmol), bromine-terminated magnetic nanoparticles (Fe_3O_4@Br-MPA) macroinitiator (362.1 mg), HEMA (1.64 g, 12.6 mmol), and anisole (3.6 mL). The flask was degassed with three freeze-evacuate-thaw cycles. PMDETA (44 μL, 0.21 mmol) was deoxygenated with bubbling dry argon before injection into the reaction system by syringe. Then, the polymerization was performed at 50 °C for 4.5 h. The mixture was diluted with THF at a solution/THF volume ratio of 1:10. The final product was precipitated with methanol, separated by centrifugation, and dried *in vacuo*.

2.5. Synthesis of Fe_3O_4@PHEMA-g-PCL nanoparticles

A typical polymerization procedure was as follows: Rigidly dried Fe_3O_4@PHEMA nanoparticles (122.6 mg) were dispersed in anhydrous THF (2 mL) under argon atmosphere. Then, freshly distilled CL (150.7 mg, 1.32 mmol) was added to the mixture. After removing of THF under reduced pressure, a catalytic amount of Sn(Oct)$_2$ in anhydrous toluene was added to the mixture, and the exhausting-refilling processes was carried out to remove the toluene. The tube was put into an oil bath at 120 °C under argon atmosphere with stirring and cooled to room temperature after polymerization for 24 h. The resulting product was dissolved in chloroform and precipitated twice with methanol. The purified product was dried in a vacuum oven until constant weight.

2.6. Separation of the polymeric PHEMA-g-PCL arms from Fe_3O_4 core

A typical procedure was as follows: PHEMA-g-PCL nanoparticles (116 mg) were dispersed in dichloromethane (10 mL) in a round bottom flask with stirring, followed by addition of 1 M aqueous HCl (20 mL). The mixture was stirred vigorously at room temperature until the black color had changed to bright yellow. The organic phase was then washed with brine and dried overnight with anhydrous $MgSO_4$. After the evaporation of dichloromethane, the copolymer was purified by precipitation from hexane and dried *in vacuo* to constant weight.

2.7. In vitro degradation of Fe_3O_4@PHEMA-g-PCL nanoparticles

50 mg of Fe_3O_4@PHEMA-g-PCL nanoparticles (Sample 5 and Sample 6) and linear PCL were placed into test tube with 15 mL phosphate buffer solution (PBS, pH 7.4) at 37 °C, respectively. At present intervals, the samples were washed with distilled water, and dried *in vacuo* to constant weight at room temperature.

2.8. Drug release of Fe_3O_4@PHEMA-g-PCL nanoparticles

50 mg of Fe_3O_4@PHEMA-g-PCL nanoparticles and 2.5 mg of model drug chlorambucil were mixed with 5 mL of chloroform under nitrogen atmosphere. Residual solvent were removed *in vacuo* at room temperature for 2 days until a constant weight was obtained. Fe_3O_4@PHEMA-g-PCL nanoparticles loading chlorambucil were sealed using dialysis membrane. The membrane was immersed into 40 mL of buffer solution (pH = 7.0) at 37 °C. In a certain interval, 5.0 mL of buffer solution was withdrawn and replaced by 5.0 mL of fresh buffer solution. The chlorambucil release was measured by UV–visible spectrophotometer using 255.4 nm as characteristic band. The cumulative release was calculated by using eq (1) as follows

$$\text{Cumulative release}(\%) = 100 \times \left(40.0c_n + 5.0\sum c_{(n-1)}\right)\Big/ W_0 \quad (1)$$

where c_n (mg/mL) is the concentration of chlorambucil in buffer solution which was withdrawn for n times; c_{n-1} (mg/mL) is the concentration of chlorambucil in buffer solution which was withdrawn for $n-1$ times; W_0 (mg) is the weight of chlorambucil in Fe_3O_4@PHEMA-g-PCL nanoparticles.

3. Results and discussion

3.1. Preparation of monodisperse Fe_3O_4 nanoparticles and Fe_3O_4@Br-MPA nanoparticles macroinitiators

The TEM image of Fe_3O_4 nanoparticles was shown in Fig. 1(a). It can be seen that the monodisperse Fe_3O_4 nanoparticles present uniform sphere and the size of them is about 4 nm. In the IR spectrum [Fig. 2(a)], the peak at 586 cm^{-1} is assigned to Fe–O of Fe_3O_4 [50,51]. The content of oleic acid on the surface of Fe_3O_4 nanoparticles calculated in accordance to TGA [Fig. 3(a)] was 23.2 wt.-%. Namely, the oleic acid density was 0.82 mmol g^{-1} of oleic acid stabilized Fe_3O_4 nanoparticles.

Oleic acid stabilized Fe_3O_4 nanoparticles underwent ligand exchange with Br-MPA to gain Fe_3O_4@Br-MPA macroinitiators for ATRP. In general, the ligand exchange method is a feasible approach because the surface capping agents can be exchanged in a controllable fashion in accordance to the function groups and concentration of the surfactants [52–54]. According to the IR spectrum [Fig. 2(b)], the intensity of C–H vibration band of CH_2 asymmetric and symmetric stretch of oleic acid at 2920 cm^{-1} and 2850 cm^{-1} decreased, while the alkyl C–H vibration of CH_3 symmetric at 2963 cm^{-1} became relatively stronger than that in Fig. 2(a), which indicated that some of the oleic acid molecules were replaced by Br-MPA molecules. The value determined by TGA [Fig. 3(b)] showed the content of oleic acid and Br-MPA was 18.0 wt.% (oleic acid: 8.4% and Br-MPA: 9.6%), suggesting that there was an equilibrium in this

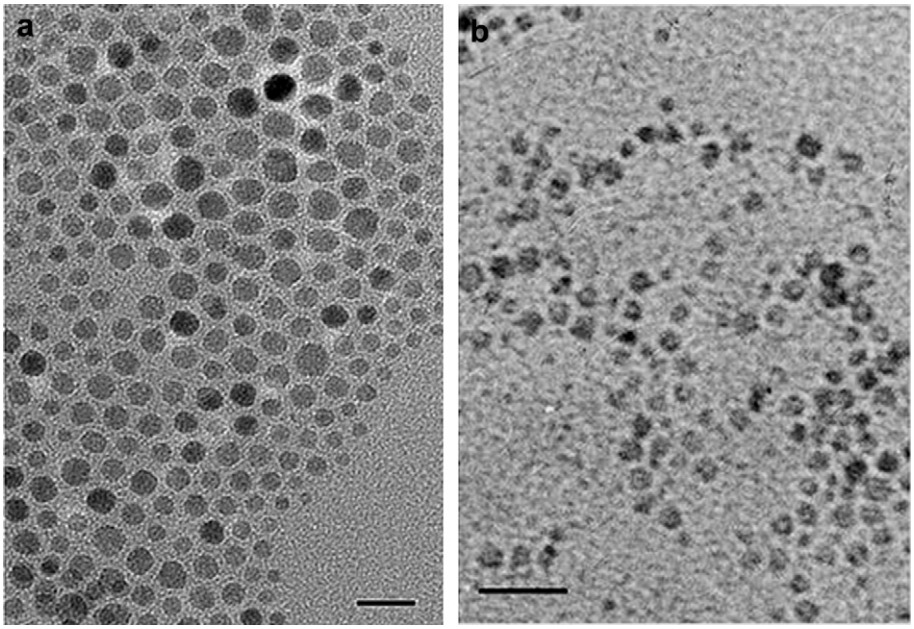

Fig. 1. TEM images of (a) oleic acid stabilized Fe_3O_4 nanoparticles and (b) Fe_3O_4@PHEMA-*g*-PCL nanoparticles. The scale bar is 20 nm.

ligand exchange process and not all oleic acid molecules were replaced from Fe_3O_4 surfaces. The Br-MPA density was 0.58 mmol g^{-1} of Fe_3O_4@Br-MPA macroinitiators after ligand exchange process.

3.2. Preparation of Fe_3O_4@PHEMA nanoparticles by ATRP

The polymerization of PHEMA was performed on the surface of Fe_3O_4 nanoparticles by ATRP in anisole at 50 °C. The weight feed ratio of HEMA monomer to Fe_3O_4@Br-MPA macroinitiator ranged from 2.26:1 to 6.04:1. The reaction time was 4.5 h. As shown in the IR spectrum [Fig. 2(c)], a novel absorption peak at 1716 cm^{-1} was assigned to the carbonyl band of PHEMA, which indicated the successful synthesis of PHEMA on the surfaces of Fe_3O_4 nanoparticles. As for the molecular weight of PHEMA, we used dilute hydrochloric acid to try to separate polymers from the particles [29,54]. However, PHEMA polymer can not be precipitated from solvent. We tried to remove the solvent directly and measure the molecular weight of PHEMA by GPC, but no obvious signal can be found due to the very low molecular weight of PHEMA. The fact can be explained as follows. In order to avoid the obvious decrease of magnetic force, the polymeric layer can not be designed to too thick. Therefore, the chain-length of PHEMA is short in the polymeric layer. The molecular weight of PHEMA should be low. As a result, it is difficult to collect PHEMA polymer with very low molecular weight and to measure the molecular weight by GPC. Nevertheless, in this work, the PHEMA with short chains is just what we needed. We needn't the PHEMA with long chains here.

The TGA data could further demonstrated the content of PHEMA on the surface of Fe_3O_4 nanoparticles. According to the data of Table 1 and TGA [Fig. 3(c)], the content of PHEMA (excluding the content of Br-MPA molecules) increased from 6.5 to 13.8 wt.-% as the weight feed ratio (R_{wt}) rose from 2.26:1 to 6.04:1. Take Sample 2

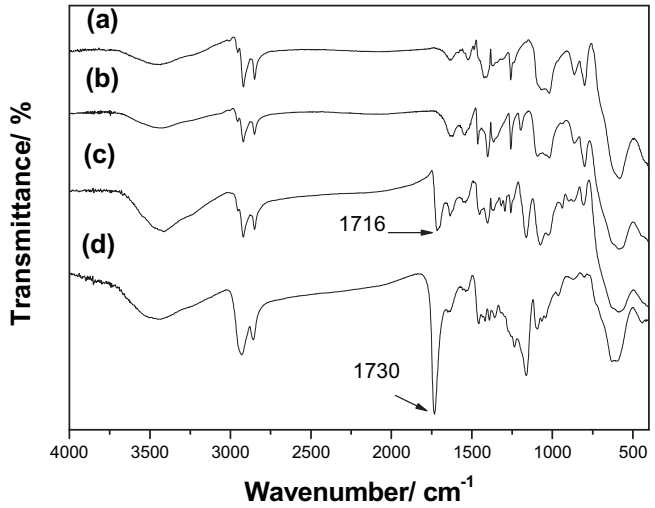

Fig. 2. IR spectra of (a) oleic acid stabilized Fe_3O_4, (b) Fe_3O_4@Br-MPA, (c) Fe_3O_4@PHEMA, and (d) Fe_3O_4@PHEMA-*g*-PCL nanoparticles.

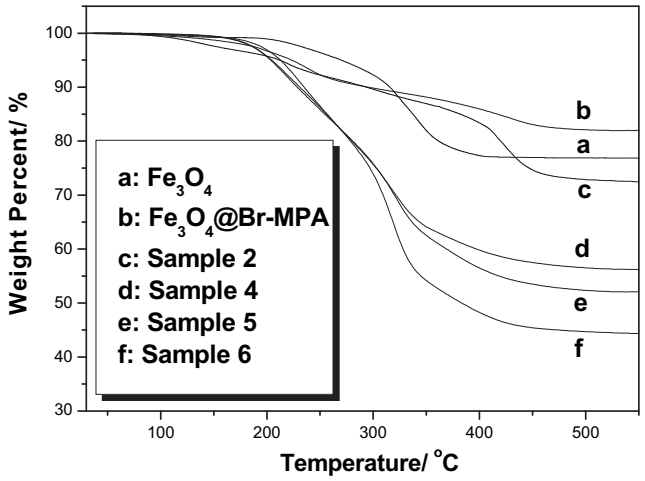

Fig. 3. TGA thermograms of (a) oleic acid stabilized Fe_3O_4, (b) Fe_3O_4@Br-MPA, (c) Fe_3O_4@PHEMA (Sample 2), and (d–f) Fe_3O_4@PHEMA-*g*-PCL nanoparticles (Sample 4–6).

Table 1
Reaction conditions and results for ATRP of HEMA on the surface of Fe_3O_4 nanoparticles.

Sample	R_{wt}[a]	R_{mol}[b]	Temp./°C	Time/h	$PHEMA_{wt.-\%}$[c]
1	2.26:1	30:1:1	50	4.5	6.5
2	4.53:1	60:1:1	50	4.5	11.7
3	6.04:1	80:1:1	50	4.5	13.8

[a] R_{wt} = HEMA:Fe_3O_4@Br-MPA (wt:wt).
[b] R_{mol} = HEMA:CuBr:PMDETA (mol:mol:mol).
[c] $PHEMA_{wt.-\%}$ = PHEMA content of the Fe_3O_4@PHEMA nanoparticles calculated from TGA data (excluding the content of Br-MPA molecules).

in Table 1 for example, the density of hydroxyl groups in PHEMA was 0.9 mmol g^{-1} of Fe_3O_4@PHEMA nanoparticles. The presence of hydroxyl groups at the side chain of PHEMA could further initiate the polymerization of CL.

3.3. Preparation of Fe_3O_4@PHEMA-g-PCL nanoparticles by ROP

The Fe_3O_4@PHEMA-*g*-PCL nanoparticles were prepared by the reaction of Fe_3O_4@PHEMA with CL in the presence of a catalytic amount of $Sn(Oct)_2$ at 120 °C by bulk polymerization. The hydroxyl groups in PHEMA segments can initiate ROP of CL. As for COOH groups at the surface of Fe_3O_4, due to the presence of interaction of COOH and Fe_3O_4, and the shield effect of PHEMA, there are not effects of COOH groups on the polymerization process. The TEM image of the Fe_3O_4@PHEMA-*g*-PCL nanoparticles is shown in Fig. 1

Table 2
Results of the polymerization[a] of Fe_3O_4@PHEMA nanoparticles initiator (Sample 2) with CL in bulk by ROP.

Sample	R_{wt}[b]	DP[c]	$M_{n,\ GPC}$[d]	PDI[d]	$PCL_{wt.-\%}$
4	0.82:1	8	6400	1.24	22.4
5	1.23:1	11	8100	1.19	28.1
6	2.46:1	18	12 900	1.22	38.8

[a] Reaction conditions: [CL]/[$Sn(Oct)_2$] = 1000; polymerization time = 24 h; polymerization temperature = 120 °C.
[b] R_{wt} = CL:Fe_3O_4@PHEMA (wt:wt).
[c] DP denotes the average degree of polymerization of PCL segments as determined by ^{1}H NMR.
[d] $M_{n,\ GPC}$ and PDI of PHEMA-*g*-PCL copolymers that separated from Fe_3O_4 core were determined by GPC analysis.

(b). The nanoparticles could be dispersed in organic solvent such as THF and dichloromethane. The existence of PCL segments in Fe_3O_4@PHEMA-*g*-PCL nanoparticles could be confirmed by IR spectrum. According to Fig. 2(c), the intensive carbonyl band absorption peak at 1730 cm^{-1} should be assigned to the carbonyl band of PCL segments. Three experiments with different feed ratio of CL to Fe_3O_4@PHEMA nanoparticles (Sample 2) were carried out. The corresponding PCL segments content of the Fe_3O_4@PHEMA-*g*-PCL nanoparticles determined by TGA were displayed in Fig. 3(d–f) and Table 2. The grafted PCL segments content increased from 22.4 to 38.8 wt.-% as the weight feed ratio (R_{wt}) rose from 0.82:1 to 2.46:1.

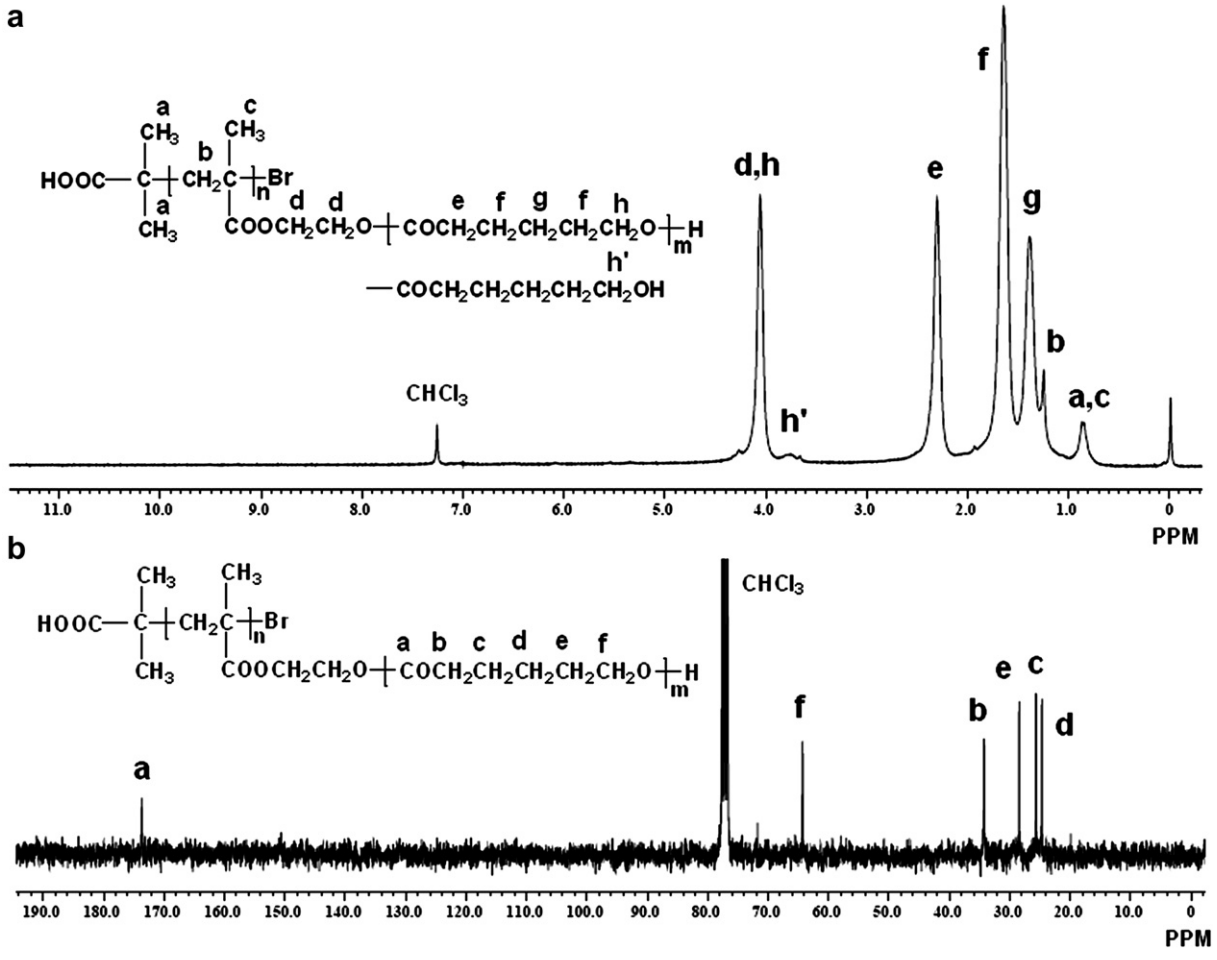

Fig. 4. (a) ^{1}H NMR and (b) ^{13}C NMR spectra of PHEMA-*g*-PCL arms separated from Fe_3O_4 core.

To make ^{1}H NMR, ^{13}C NMR, and GPC samples, the polymeric PHEMA-*g*-PCL arms were separated from Fe_3O_4@PHEMA-*g*-PCL nanoparticles through acidolysis of Fe_3O_4 with dilute hydrochloric acid. The degradation of PCL did not happen during the separation of polymeric shell from the particles using acid according the literatures [29,54]. A typical ^{1}H NMR spectrum of the copolymer PHEMA-*g*-PCL with the assignment is presented in Fig. 4(a). The major resonance peaks (a–h) have been attributed to PCL and PHEMA (including Br-MPA). The proton signal (peak h') is assigned to the terminated methylene of PCL segments. The average degree of polymerization (DP) for the PCL segments was calculated by ^{1}H NMR from the integration of the signals of methylene protons (peak e) to the terminal methylene protons (peak h'). Because not all the HEMA units were linked to a PCL chain, so in fact, the DP of the PCL is an average value. The DP of PCL segments was increased from 8 to 18 as the weight feed ratio (R_{wt}) rose from 0.82:1 to 2.46:1. Fig. 4(b) shows the ^{13}C NMR spectrum and the assignment for PCL segments. The expected peaks attributed to PCL (peaks a-f) can be clearly detected, and there is only one peak for the carbonyl of PCL (peak a), which indicates that the transesterification reaction of PCL did not occur during the synthesis of Fe_3O_4@PHEMA-*g*-PCL nanoparticles. The molecular weight distributions (PDI) of the PHEMA-*g*-PCL copolymers are narrow in accordance to the data of GPC (Table 2), which indicates that the synthesis of Fe_3O_4@PHEMA-*g*-PCL nanoparticles by ATRP and ROP under the aforementioned conditions could be well controlled.

3.4. Thermal and magnetic properties of Fe_3O_4@PHEMA-g-PCL nanoparticles

The thermal properties of Fe_3O_4@PHEMA-*g*-PCL were investigated with DSC and compared with those of the linear counterpart. Table 3 shows data for the thermal properties of some samples. According to the DSC data, the melting point (T_m) and degree of crystallinity (X_c) of Fe_3O_4@PHEMA-*g*-PCL were lower than those of linear PCL and increased with the length of the PCL segments. This was attributed to the crystalline imperfection mainly due to the short chain length of the PCL segments of Fe_3O_4@PHEMA-*g*-PCL. Moreover, the branched structure of the PHEMA-*g*-PCL on the surfaces of Fe_3O_4 nanoparticles led to the steric hindrance and made a contribution to the imperfection. As shown in Fig. 5 and Table 3, T_m and X_c of PCL segments of Fe_3O_4@PHEMA-*g*-PCL (Sample 5) were 43.9 °C and 6.8%, respectively, whereas T_m and X_c of the linear PCL were 56.1 °C and 51.3%.

The magnetic properties of oleic acid Fe_3O_4 and Fe_3O_4@PHEMA-*g*-PCL nanoparticles were investigated on a vibrating sample magnetometer system at room temperature. Fig. 6 shows the magnetization curves of oleic acid Fe_3O_4 and Fe_3O_4@PHEMA-*g*-PCL nanoparticles (Sample 5). These particles don't exhibit obvious hysteresis at low magnetic field and room temperature. Moreover, these particles shows superparamagnetism because the diameter

Table 3
Thermal properties and crystallinity data for the PCL segments of Fe_3O_4@PHEMA-*g*-PCL nanoparticles.

Sample[a]	T_m (°C)[b]	ΔH (J g^{-1})[c]	X_c (%)[d]
4	41.7	5.1	3.7
5	43.9	9.2	6.8
6	47.9	19.8	14.5
Linear PCL	56.1	69.8	51.3

[a] The samples (4–6) are the same as those in Table 2. M_n of Linear PCL was 5800.
[b] Melting points of PCL segments.
[c] Heat of melting of crystalline PCL segments.
[d] Degree of crystalline PCL segments calculated from the heat of melting with a heat of 136.1 J/g for 100% crystalline PCL.

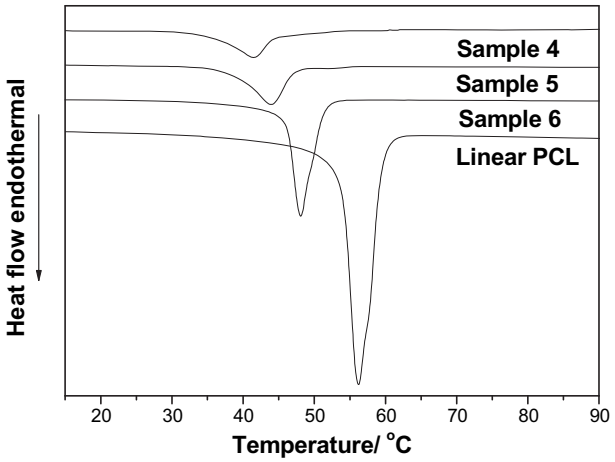

Fig. 5. DSC curves of linear PCL, and Fe_3O_4@PHEMA-*g*-PCL nanoparticles (Sample 4–6).

of these Fe_3O_4 nanoparticles (about 4 nm) is much less than the critical particle size of ferromagnetism of Fe_3O_4 nanoparticles (25 nm) [55]. The saturation magnetization of Fe_3O_4@PHEMA-*g*-PCL nanoparticles (Sample 5) (14.4 A·m^2/kg) is less than that of oleic acid stabilized Fe_3O_4 (27.8 A·m^2/kg), which should be attributed to the presence of PHEMA-*g*-PCL copolymer coated on the surface of Fe_3O_4 nanoparticles.

3.5. In vitro degradation properties of Fe_3O_4@PHEMA-g-PCL nanoparticles

The degradation behavior of PCL segments in Fe_3O_4@PHEMA-*g*-PCL nanoparticles and linear PCL were investigated by immersing them in pH 7.4 PBS at 37 °C. The weight loss of PCL segments in linear PCL and Fe_3O_4@PHEMA-g-PCL nanoparticles during degradation period are shown in Fig. 7. The degradation rate of linear PCL was very slow. For example, the weight loss was 2.1% after degradation for 30 days. This should be attributed to the high degree of crystallinity of linear PCL. The degradation rate of PCL segments in Fe_3O_4@PHEMA-g-PCL nanoparticles was obviously faster than that of linear PCL and increased with the decrease of the length of PCL chains. For instance, the weight loss of Sample 5 was 5.8% after degradation for 30 days. This should be ascribed to the relatively low degree of crystallinity of PCL chains in Fe_3O_4@PHEMA-g-PCL

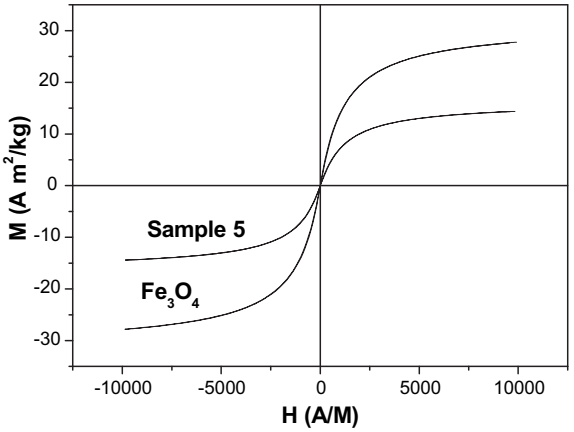

Fig. 6. Magnetic curves of oleic acid stabilized Fe_3O_4 nanoparticles and Fe_3O_4@PHEMA-*g*-PCL nanoparticles (Sample 5) at room temperature.

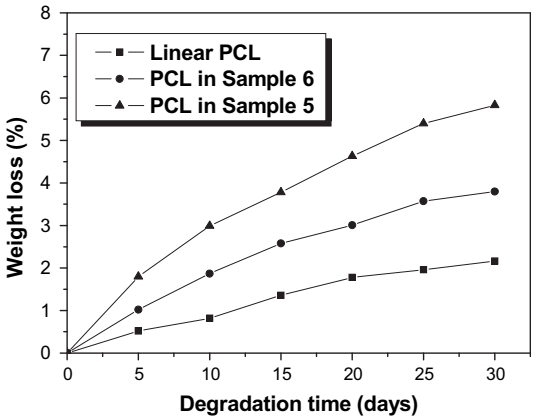

Fig. 7. Degradation behavior of PCL chains in Fe_3O_4@PHEMA-*g*-PCL nanoparticles (Sample 5 and Sample 6) and linear PCL.

nanoparticles. The degradation of polyester has been shown to take place by random hydrolysis of ester bonds. The PCL segments in Fe_3O_4@PHEMA-g-PCL nanoparticles possessed a branched structure which led to the decrease of crystallinity and the increase of the rate of amorphousness of PCL. Therefore, the water molecule pervaded the molecules of PCL in Fe_3O_4@PHEMA-g-PCL nanoparticles was faster than that of linear PCL, which promoted the hydrolytic degradation of PCL segments.

3.6. Drug release of Fe_3O_4@PHEMA-g-PCL nanoparticles

PCL presents good drug permeability and therefore Fe_3O_4@-PHEMA-*g*-PCL nanoparticles could be expected to become a carrier in drug release system. Chlorambucil was a kind of anticancer agent and used as a model drug to investigate the release properties of Fe_3O_4@PHEMA-*g*-PCL nanoparticles. Moreover, chlorambucil is a kind of hydrophobic drug and can be encapsulated into PHEMA-g-PCL polymeric layer. Therefore, drug was released from polymeric layer by diffusion pattern. The release experiments were carried out under the condition of pH 7.0 at 37 °C. The cumulative release of chlorambucil from loading Sample 4 and Sample 6 was presented in Fig. 8. As shown in Fig. 8, the release rate of Sample 4 was faster than that of Sample 6. This should be attributed to the PCL polymer layer in Sample 4 was thinner than that in Sample 6. As a result, chlorambucil in Sample 6 was more difficult in diffusing out from PCL polymer layer than that in Sample 4. Obviously, the rate of drug release could be adjusted by altering the length of PCL chains in Fe_3O_4@PHEMA-*g*-PCL nanoparticles.

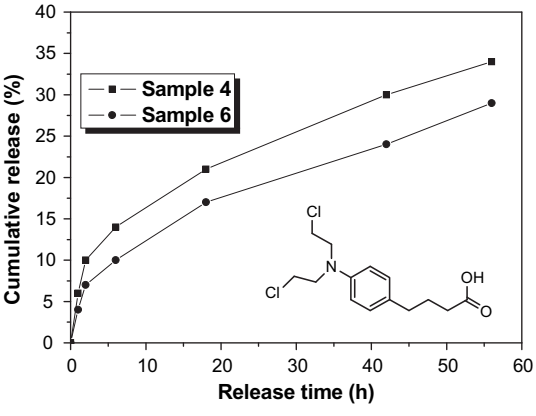

Fig. 8. Release profiles of chlorambucil from Fe_3O_4@PHEMA-*g*-PCL nanoparticles (Sample 4 and Sample 6) under the conditions of pH 7.0 at 37 °C.

4. Conclusions

A series of novel well-defined Fe_3O_4@PHEMA-*g*-PCL magnetic nanoparticles with branched brush polymeric shell were successfully synthesized by combination of ATRP and ROP. Fe_3O_4@Br-MPA was prepared by ligand exchange of monodisperse Fe_3O_4 with Br-MPA. Then, Fe_3O_4@PHEMA was synthesized by ROP of HEMA with Br-MPA macroinitiator. Finally, PCL segments were grafted from the side of PHEMA by the ROP of CL with the hydroxyl groups of the PHEMA segments used as initiation centers, and Fe_3O_4@PHEMA-*g*-PCL magnetic nanoparticles were obtained. The PCL segments of Fe_3O_4@PHEMA-*g*-PCL possessed lower crystallinity than those of linear PCL. *In vitro* degradation investigation indicated that the degradation rate of PCL segments in Fe_3O_4@PHEMA-*g*-PCL increased with the decrease of the length of PCL chains. The release behavior of chlorambucil from the nanoparticles indicated that the rate of drug release could be adjusted by altering the length of PCL chains in Fe_3O_4@PHEMA-*g*-PCL nanoparticles. The nanoparticles have potential applications in bionanomaterials, biosensor, and biomedical fields. The synthesis method for branched brush polymeric shell developed here can be extended to prepare more kinds of inorganic/organic hybrid nanomaterials and improve the functions.

Acknowledgements

The authors gratefully acknowledge the financial support of the National Natural Science Foundation of China (no. 20836004, and 20974058), and the National Basic Research Program of China (2009CB930602).

References

[1] Vestal CR, Zhang ZJ. J Am Chem Soc 2002;124(48):14312–3.
[2] White MA, Johnson JA, Koberstein JT, Turro NJ. J Am Chem Soc 2006;128(35):11356–7.
[3] Mandal TK, Fleming MS, Walt DR. Nano Lett 2002;2(1):3–7.
[4] Burke NAD, Stover HDH, Dawson FP. Chem Mater 2002;14(11):4752–61.
[5] Wan SR, Huang JS, Yan HS, Liu KL. J Mater Chem 2005;15(2):298–303.
[6] Li C, Benicewicz BC. Macromolecules 2005;38(14):5929–36.
[7] Lutz JF, Stiller S, Hoth A, Kaufner L, Pison U, Cartier R. Biomacromolecules 2006;7(11):3132–8.
[8] Cui T, Zhang JH, Wang JY, Cui F, Chen W, Xu FB, et al. Adv Funct Mater 2005;15(3):481–6.
[9] Barbey R, Lavanant L, Paripovic D, Schuwer N, Sugnaux C, Tugulu S, et al. Chem Rev 2009;109(11):5437–527.
[10] Viswanathan K, Ozhalici H, Elkins CL, Heisey C, Ward TC, Long TE. Langmuir 2006;22(3):1099–105.
[11] Yuan JJ, Schmid A, Armes SP, Lewis AL. Langmuir 2006;22(26):11022–7.
[12] Giacalone F, Martin N. Chem Rev 2006;106(12):5136–90.
[13] Li DJ, Sheng X, Zhao B. J Am Chem Soc 2005;127(17):6248–56.
[14] Kang Y, Taton TA. Macromolecules 2005;38(14):6115–21.
[15] Yang L, Luo YF, Jia XR, Ji Y, You LP, Zhou QF, et al. J Phys Chem B 2004;108(4):1176–8.
[16] Guo J, Yang WL, Wang CC, He J, Chen JY. Chem Mater 2006;18(23):5554–62.
[17] Zhou M, Yuan JY, Yuan WZ, Yin YW, Hong XY. Nanotechnology 2007;18(40):405704.
[18] Zhou LL, Yuan WZ, Yuan JY, Hong XY. Mater Lett 2008;62(9):1372–5.
[19] Zhang XW, Yang YF, Tian J, Zhao HY. Chem Commun 2009;25:3808–9.
[20] Guo ZP, Chen YW, Zhou WH, Huang ZF, Hu YH, Wan MX, et al. Mater Lett 2008;62:4542–4.
[21] Lee DK, Kang YS, Lee CS, Stroeve P. J Phys Chem B 2002;106(29):7267–71.
[22] Yang TZ, Shen CM, Li Z, Zhang HR, Xiao CW, Chen ST, et al. J Phys Chem B 2005;109(49):23233–6.
[23] Caruntu D, Caruntu G, Chen Y, O'Connor CJ, Goloverda G, Kolesnichenko VL. Chem Mater 2004;16(25):5527–34.
[24] Zhang DH, Liu ZQ, Han S, Li C, Lei B, Stewart MP, et al. Nano Lett 2004;4(11):2151–5.
[25] Tan ST, Wendorff JH, Pietzonka C, Jia ZH, Wang GQ. Chem Phys Chem 2005;6(8):1461–5.
[26] Garcia I, Zafeiropoulos NE, Janke A, Tercjak A, Eceiza A, Stamm M, et al. J Polym Sci Part A Polym Chem 2007;45(5):925–32.

[27] Wang PC, Lee CF, Young TH, Lin DT, Chiu WY. J Polym Sci Part A Polym Chem 2005;43(7):1342–56.
[28] Liao MH, Chen DH. J Mater Chem 2002;12(12):3654–9.
[29] Schmidt AM. Macromol Rapid Commun 2005;26(1):93–7.
[30] Gelbrich T, Feyen M, Schmidt AM. Macromolecules 2006;39(9):3469–72.
[31] Wang WC, Neoh KG, Kang ET. Macromol Rapid Commun 2006;27 (19):1665–9.
[32] Bai YP, Teng B, Chen SZ, Chang Y, Li ZL. Macromol Rapid Commun 2006;27 (24):2107–12.
[33] Zhou LL, Yuan JY, Yuan WZ, Zhou M, Wu SZ, Li ZL, et al. Mater Lett 2009;63 (18/19):1567–70.
[34] Zhou LL, Yuan JY, Yuan WZ, Sui XF, Wu SZ, Li ZL, et al. J Magn Magn Mater 2009;321(18):2799–804.
[35] Albertsson AC, Varma IK. Biomacromolecules 2003;4(6):1466–86.
[36] Jeong SI, Kim BS, Lee YM, Ihn KJ, Kim SH, Kim YH. Biomacromolecules 2004;5 (4):1303–9.
[37] Wang JL, Wang L, Dong CM. J Polym Sci Part A Polym Chem 2005;43 (22):5449–57.
[38] Fay F, Linossier I, Langlois V, Renard E, Vallee-Rehel K. Biomacromolecules 2006;7(3):851–7.
[39] Miao ZM, Cheng SX, Zhang XZ, Zhuo RX. Biomacromolecules 2006;7 (6):2020–6.
[40] Srivastava RK, Albertsson AC. Biomacromolecules 2006;7(9):2531–8.
[41] Rosenberg R, Devenney W, Siegel S, Dan N. Mol Pharmaceutics 2007;4 (6):943–8.
[42] Yuan WZ, Yuan JY, Zhang FB, Xie XM. Biomacromolecules 2007;8(1):1101–8.
[43] Yuan WZ, Yuan JY, Zhang FB, Xie XM, Pan CY. Macromolecules 2007;40 (25):9094–102.
[44] Yan Q, Yuan JY, Zhang FB, Sui XF, Xie XM, Yin YW, et al. Biomacromolecules 2009;10(8):2033–42.
[45] Zhao HY, Kang XL, Liu L. Macromolecules 2005;38(26):10619–22.
[46] Yu WH, Kang ET, Neoh KG. Langmuir 2005;21(1):450–6.
[47] Yang Q, Tian J, Hu MX, Xu ZK. Langmuir 2007;23(12):6684–90.
[48] Moglianetti M, Campbell RA, Nylander T, Varga I, Mohanty B, Claesson PM, et al. Soft Matter 2009;5(19):3646–56.
[49] Sun SH, Zeng H, Robinson DB, Raoux S, Rice PM, Wang SX, et al. J Am Chem Soc 2004;126(1):273–9.
[50] Yuan JJ, Armes SP, Takabayashi Y, Prassides K, Leite CAP, Galembeck F, et al. Langmuir 2006;22(26):10989–93.
[51] Sun J, Zhou SB, Yang Y, Weng J, Li XH, Li MY. J Biomed Mater Res Part A 2007;80A(2):333–41.
[52] Boal AK, Das K, Gray M, Rotello VM. Chem Mater 2002;14(6):2628–36.
[53] Bourlions AB, Bakandritsos A, Georgakilas V, Petridis D. Chem Mater 2002;14 (8):3226–8.
[54] Wang Y, Teng XW, Wang JS, Yang H. Nano Lett 2003;3(6):789–93.
[55] Lee J, Isobe T, Senna MJ. Colloid Interface Sci 1996;177(2):490–4.